This article has been accepted for publication in Journal of Lightwave Technology. This is the author's version which has not been fully edited and content may change prior to final publication. Citation information: DOI 10.1109/JLT.2026.3748590

Telecommunication Cable Fault Positioning Based on Synchronization-free Time-Delay Method

Shangwei Dai, Hanjie Liu, Xing Rao, Danxia Lu, Linqiao Du, Qiji Ma, Guoqiang Liu, Junhong Lu, Junmin Liu, Guoxiang Xu, Rendong Xu, Yiping Wang, and George Y. Chen

***Abstract*—With the rapid development of internet-based services, there is an urgent need for intelligent monitoring and management of global optical networks. Long-haul optical backbone networks are susceptible to fiber breaks caused by natural and manmade factors, leading to inconvenient service interruptions and economic losses. Conventional monitoring techniques such as phase-sensitive optical time-domain reflectometry (Φ-OTDR) are limited due to the need for dedicated hardware (laser, repeaters and detectors), occupies communication bandwidth and exhibits pulse distortion post-amplification. To overcome these limitations, we propose a synchronization-free bidirectional time-difference method for break point positioning, which derives the fault location from the time difference between the bidirectional intensity-loss moments of the received communication signal itself. Differences in local time between the two detection ends are cancelled out via a one-time controlled break point positioning as calibration. This approach inherently resolves the key problem of unsynchronized data acquisition between the two ends of a long-haul link, eliminating the need for dedicated sensing hardware (other than a simple photodetector and data acquisition module), separate monitoring wavelengths, or any extra synchronization mechanisms. For precise identification of the intensity-loss moments, an envelope-guided optimal change-point detection algorithm is then employed. The experimental results demonstrate that over a 100 km fiber link (limited only by the available communication cable length) with relay amplification, the proposed method can achieve an RMSE of 8.0 m relative to the true break position and an STD of 6.1 m over repeated measurements by using the intensity-loss moments of the data-encoded signal. Moreover, the practical effectiveness of the proposed method is validated through successful fiber break point detection using off-the-shelf commercial transceivers.**

***Index Terms*—Break point positioning, optical cable, bidirectional time-difference, change-point detection.**

I. INTRODUCTION

In recent years, driven by the rapid advancement of Internet-based services such as cloud computing [1], the Internet of Things (IoT) [2], virtual reality [3], and particularly large AI models [4], global optical communication networks have been undergoing exponential growth. There is a growing imperative for intelligent monitoring and management of large-scale in-service optical networks, particularly urban optical backbone networks [5]. These optical networks extend hundreds to thousands of kilometers, supported by multiple repeater stations, and are often deployed in remote areas. As a result, they are prone to natural disasters such as landslides [6] and earthquakes [7], which can cause fiber breaks and thus abrupt data termination. Such damage severely disrupts data transmission in metropolitan and access networks, even lead to large-scale service outages. Consequently, fast and precise positioning of break locations along long-distance optical fibers or cables can lead to faster repair and significantly reduces the associated economic impact [8].

The optical time-domain reflectometer (OTDR) has long been the standard tool for fiber fault positioning, but it faces fundamental limitations in long-haul backbone networks with inline amplifiers [9]. First, erbium-doped fiber amplifiers (EDFAs) and isolators interrupt the backscattered and reflected light on which OTDR relies, making it inoperative across multiple repeater spans. Second, although a dedicated maintenance wavelength (e.g., 1650 nm) has been standardized for OTDR operation to avoid interference with data channels [10], deploying such a scheme still requires additional laser sources, detectors, and wavelength-division multiplexing components at both ends, increasing system complexity and cost. The dedicated wavelength is taken from potential communication bandwidth. Third, EDFAs are optimized for communication signals and inevitably distort the OTDR probe pulses, degrading sensing accuracy [26]. Attempts to overcome these issues by modifying the network infrastructure or adding extra optical channels have been proposed [11-15], but they increase complexity and are incompatible with existing fiber links.

As an alternative to backscattering-based distributed fiber optic sensing systems, forward-transmission vibration sensing

This research is supported by National Natural Science Foundation of China (W2532046, 62275172, U22A2088); Shenzhen Science and Technology Program (JCYJ20241202124408012, JCYJ20220818095800001); Shenzhen Key Laboratory of Ultrafast Laser Micro-Nano Manufacturing (ZDSYS20220606100405013); Research Team Cultivation Program of Shenzhen University (2023DFT001). (*Corresponding author: George Y. Chen*)

Shangwei Dai, Hanjie Liu, Xing Rao, Danxia Lu, Linqiao Du, Qiji Ma, Guoqiang Liu, Junhong Lu, Yiping Wang and George Y. Chen are with State Key Laboratory of Radio Frequency Heterogeneous Integration, Key Laboratory of Optoelectronic Devices and Systems of Ministry of Education and Guangdong Province, College of Physics and Optoelectronic Engineering, Shenzhen University, Shenzhen 518060, Guangdong Province, P. R. China, and are also with Shenzhen Key Laboratory of Ultrafast Laser Micro/Nano Manufacturing, Guangdong and Hong Kong Joint Research Centre for Optical Fibre Sensors, Shenzhen University, Shenzhen 518060, Guangdong Province, P. R. China. (email: 2350453003@email.szu.edu.cn; liuhanjie@szu.edu.cn; raoxing@szu.edu.cn; 3236507616@qq.com; 2453232013@mails.szu.edu.cn; 937198205@qq.com; 2400233054@mails.szu.edu.cn; 241023076@mails.szu.edu.cn; ypwang@szu.edu.cn; gychen@szu.edu.cn)

Junmin Liu is with College of New Materials and New Energies, Shenzhen Technology University, Shenzhen 5l8118, China. (email: liujunmin@sztu.edu.cn)

Guoxiang Xu and Rendong Xu are with HMN TECHNOLOGIES GROUP CO.,LTD, Suzhou, Jiangsu, 215500, China; Jiangsu Key Laboratory for Subsea Communications and Sensing, Suzhou, Jiangsu, 215500, China. (email: xugx@hmntech.com; xurd@zju.edu.cn)

Authorized licensed use limited to: SHENZHEN UNIVERSITY. Downloaded on November 16,2026 at 08:26:42 UTC from IEEE Xplore. Restrictions apply.
© 2026 IEEE. All rights reserved, including rights for text and data mining and training of artificial intelligence and similar technologies. Personal use is permitted, but republication/redistribution requires IEEE permission. See https://www.ieee.org/publications/rights/index.html for more information.

This article has been accepted for publication in Journal of Lightwave Technology. This is the author's version which has not been fully edited and content may change prior to final publication. Citation information: DOI 10.1109/JLT.2026.3748590

systems enable longer sensing distances and can be more readily integrated with existing communication systems [16,17]. Therefore, fiber break point positioning using forward-transmission light is particularly suitable for fiber fault diagnosis and positioning in long-haul optical backbone networks. Rosher et al. proposed a method using bit counting at the transceivers at both ends to locate fiber break points [18], and Zernon et al. subsequently evaluated the positioning error of this method under different fiber stress conditions [19]. Such methods offer a wider dynamic range compared with OTDR-based approaches. However, they rely on precise time synchronization. The proposed method in this work uses forward transmitted light that does not require both detection ends to be synchronized, which is a significant advantage for geographically distanced installations.

To overcome this challenge while retaining all the advantages of forward-transmission sensing, we propose a synchronization-free fiber break point positioning method based on the intensity signature of bidirectionally transmitted communication signals. First, the method extracts the break-induced intensity-loss moments from the communication signal itself, eliminating any need for dedicated sensing hardware (other than a simple photodetector and data acquisition module) or separate monitoring channels. Second, it uses the break event as an intrinsic synchronization reference to eliminate the initial acquisition time offset between the two ends, thus enabling positioning without external triggers or complex synchronization protocols. Finally, an envelope-guided optimal change-point detection algorithm is introduced to pinpoint the intensity-loss moment with high accuracy and speed. We successfully demonstrate the method on a fiber break point detection testbed using standard commercial transceivers, validating its practical effectiveness.

II. Theory

A. Fiber break point positioning method

Fig. 1 shows the basic structure of the fiber break point (BP) positioning method implemented in a communication link. At both ends, each transponder unit integrates a laser and a photodetector (PD), there are no specific requirements on the laser linewidth or polarization. The continuous optical wave emitted by the laser serves as the carrier for the communication signal encoding and is coupled into the optical fiber for transmission. Upon reaching the repeater station (RS), the optical signal is amplified by two independent erbium-doped fiber amplifiers (EDFAs) handling opposite transmission directions. The amplified optical signal is then directed through fiber termination box (FTB), for initial calibration purpose, into the transponder unit at the opposite end.

When a fiber break occurs at a point Z along the fiber, the optical power received at the photodetector abruptly drops to zero in the ideal case, though in practice there is weak background noise. Let t_{b1} and t_{b2} denote the time instants at which the abrupt decrease in the intensity signals I_1 and I_2 is detected at Transponder 1 and Transponder 2, respectively. Accordingly, $t_1 = Zn/c$ and $t_2 = (L - Z)\, n/c$ represent the propagation times of the optical field from point Z to transponder1 and transponder2, respectively, where L is the length of fiber, n is the refractive index of single mode fiber and c is the speed of light in a vacuum. Assuming the signal acquisition at both transponders is synchronized, the following simplistic relationship holds:

$$\Delta t = t_{b1} - t_{b2} = t_1 - t_2 = \frac{Zn}{c} - \frac{(L-Z)n}{c} = \frac{2Zn}{c} - \frac{Ln}{c} \tag{1}$$

$$Z = \frac{c\Delta t}{2n} + \frac{L}{2} \tag{2}$$

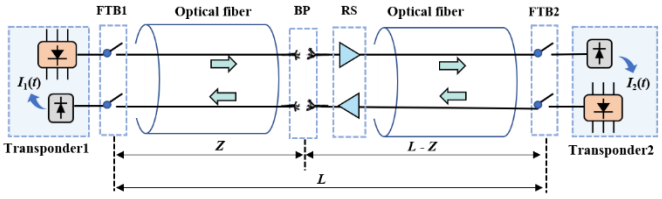


Fig. 1. Schematic of the fiber break point position in a fiber communication link. BP: fiber break point; FTB: fiber termination box; RS: repeater station.

Therefore, under ideal synchronized timing between the two transponders, the location of the fiber BP Z can be determined by monitoring the abrupt intensity-loss and obtaining the timestamps t_{b1} and t_{b2}. However, in a long-distance bidirectional transmission system [20], time synchronization typically relies on satellite-based timing [21] or dedicated fiber-based timing [22]. The satellite-based approach suffers from weak signal strength, susceptibility to interference and spoofing, and potential strategic dependency risks. The fiber-based method, meanwhile, requires the deployment of additional dedicated fiber lines. Both approaches inevitably increase the system cost and complexity.

The complete workflow of the proposed fiber BP positioning method is illustrated in Fig. 2. Assuming a time offset of t_s exists between the two transponders due to differences in their local clocks and detection-system processing delays, the fiber is intentionally disconnected at FTB1 near Transponder 1 for calibration. The corresponding intensity-loss moments detected from I_1 and I_2 are denoted as t_{c1} and t_{c2}, respectively. Since the calibration disconnection occurs near Transponder 1, the intensity loss is detected first at I_1 and subsequently at I_2 after the full-link propagation delay t_L. Therefore, the time offset t_s can be expressed as:

$$t_s = t_{c1} - t_{c2} + t_L \tag{3}$$

where $t_L = nL/c$ is defined as the propagation time of the optical signal through the fiber. In practical field deployment, the calibration process described above can be conveniently implemented by integrating a high-speed electro-optic MZI (Mach-Zehnder interferometer) switch at the FTB1 [28]. Upon receiving a single electrical trigger signal, such a switch simultaneously interrupts both the forward and return optical paths at the identical physical location with a switching time on the order of nanoseconds. The calibration does not need to

Authorized licensed use limited to: SHENZHEN UNIVERSITY. Downloaded on November 16,2026 at 08:26:42 UTC from IEEE Xplore. Restrictions apply.
© 2026 IEEE. All rights reserved, including rights for text and data mining and training of artificial intelligence and similar technologies. Personal use is permitted, but republication/redistribution requires IEEE permission. See https://www.ieee.org/publications/rights/index.html for more information.

This article has been accepted for publication in Journal of Lightwave Technology. This is the author's version which has not been fully edited and content may change prior to final publication. Citation information: DOI 10.1109/JLT.2026.3748590

be repeated before every fiber-break event. Within a continuous monitoring session, a single calibration can be reused provided that the relative timebase between the two acquisition systems and the effective propagation delay of the link remain sufficiently stable. After the initial calibration, the system operates in a passive monitoring mode, and no additional traffic interruption is introduced by the calibration during routine network operation.

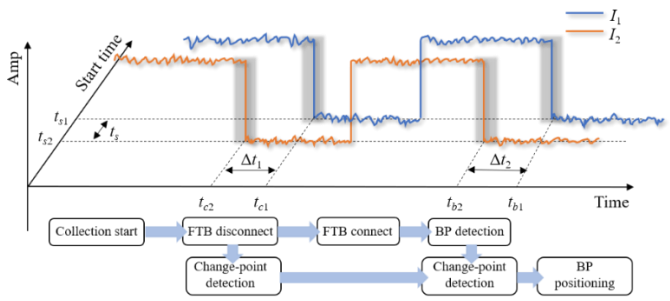


Fig. 2. Complete workflow of the fiber BP positioning method. FTB: fiber termination box, BP: fiber break point.

Consequently, at the moment a real fiber break occurs at an arbitrary position, the actual time difference of the break event Δt, as detected at the two ends can be derived from the following equation:

$$\Delta t' = t_{b1} - t_{b2} - t_s \tag{4}$$

By substituting eq. (3) into eq. (4), it can be obtained:

$$\Delta t' = \Delta t_2 - \Delta t_1 - t_L \tag{5}$$

where $\Delta t_1 = t_{c1} - t_{c2}$, $\Delta t_2 = t_{b1} - t_{b2}$. By replacing Δt in Eq. (2) with $\Delta t'$ from Eq. (5) yields an expression for the fiber break location Z under asynchronous data acquisition at the two sites:

$$Z = \frac{c\Delta t'}{2n} + \frac{L}{2} = \frac{c\left(\Delta t_2 - \Delta t_1 - t_L\right)}{2n} + \frac{L}{2} = \frac{c\left(\Delta t_2 - \Delta t_1\right)}{2n} \tag{6}$$

Consequently, the accuracy of fiber BP positioning depends on the precise detection of the four signal loss instants: t_{c1}, t_{c2}, t_{b1} and t_{b2}. Thus, to accurately pinpoint these moments, this work proposes an envelope-guided optimal change-point detection (EGO-CPD) algorithm, tailored for detecting abrupt changes in the corresponding time series. It is important to clarify the applicable scope of the proposed method. The bidirectional time-difference formulation in Eq. 6 is derived under the essential premise that the two intensity-loss moments t_{b1} and t_{b2} originate from the same physical event that simultaneously disrupts both transmission directions—i.e., a cable-level break where the entire cable is severed at one position. This is the dominant failure mode in long-haul terrestrial and submarine optical backbone networks, where external forces such as excavation, landslides, or ship anchor drags typically damage the entire cable sheath. For the scenario where the two fibers break at different times or at different locations, the proposed method is not suitable because t_{b1} and t_{b2} no longer correspond to a common event, and the time difference Δt_2 would contain an unknown time interval between the two independent break events. For different attenuation depths or falling-edge slopes do not directly invalidate the proposed method because the loss instant is detected independently from each received waveform. However, a reduced edge steepness increases the uncertainty of change-point estimation, and asymmetric edge degradation between the two directions may introduce a differential timing bias.

B. Envelope-guided optimal change-point detection algorithm

Traditional change-point detection (CPD) algorithms such as pruned exact linear time (PELT), binary segmentation, bottom-up segmentation and window-based segmentation often scales poorly with data size, making high-resolution analysis costly. According to Eq. (6), the accuracy of fiber BP positioning depends on temporal precision. Specifically, higher temporal resolution leads to higher positioning accuracy. However, increased temporal resolution results in a corresponding rise in the number of data points, which substantially increases the computational burden of the change-point algorithm. This implies that there exists fundamental trade-off between positioning accuracy and computational load. To break free from this trade-off, an envelope-guided optimal change-point detection (EGO-CPD) algorithm is proposed. This approach significantly reduces computational load by first identifying a refined search region through envelope derivative analysis, then applying the optimal change-point detection within this confined interval.

The complete procedure of the EGO-CPD algorithm is presented in the pseudocode of Algorithm 1. The algorithm operates in two stages: First, a rapid but approximate method is employed to obtain a coarse estimate of the change-point position, which defines a narrowed search interval. The optimized search interval is defined for change-point detection by centering it on the index r of the peak derivative of the interferometric intensity envelope and setting its half-length l, resulting in a total fixed window of $2l$ points. Then, the optimal change-point detection is applied precisely within this reduced interval to detect the change point with high accuracy. The algorithm is described below:

Consider a time series: $X_{1..n}=\{x_1, x_2,\ldots, x_n\}$. A cost function $C(X_{a..b})$ needs to be defined to measure the internal inconsistency within a segment. it is typically defined as the sum of squared errors:

$$C\left(X_{a..b}\right) = \sum_{t=a}^{b}\left(x_t - \mu_{a..b}\right)^2 \tag{7}$$

In addition, a gain function $Gain(\tau)$ need to be defined to the benefit of splitting at a change point, it can be expressed as:

$$Gain(\tau) = C\left(X_{a..b}\right) - \left[C\left(X_{a..\tau}\right) + C\left(X_{\tau+1..b}\right)\right] \tag{8}$$

where $\mu_{a..b}$ is the mean value of the time series $X_{a..b}$. Next, the optimal split point within the current segment $X_{1..n}$ is identified by evaluating the gain $Gain(\tau)$ at every possible split location τ. The point yielding the maximum gain is selected as the candidate change point τ^*, which can be expressed as:

$$\tau^* = \arg\max_{\tau\in[1,n]} Gain(\tau) \tag{9}$$

Authorized licensed use limited to: SHENZHEN UNIVERSITY. Downloaded on November 16,2026 at 08:26:42 UTC from IEEE Xplore. Restrictions apply.
© 2026 IEEE. All rights reserved, including rights for text and data mining and training of artificial intelligence and similar technologies. Personal use is permitted, but republication/redistribution requires IEEE permission. See https://www.ieee.org/publications/rights/index.html for more information.

This article has been accepted for publication in Journal of Lightwave Technology. This is the author's version which has not been fully edited and content may change prior to final publication. Citation information: DOI 10.1109/JLT.2026.3748590

Algorithm 1: Envelope-guided optimal change-point detection algorithm

Input:

Optical intensity signals $I(t)$ from PD.

Initialization:

Penalty threshold: P.

Minimum segment length: L_{min} (L_{min} = 2).

Coarse range: l

$Gain_{\max} \leftarrow -\infty$, $\tau^* \leftarrow$ null

Output:

Change point sequence $T=\{\tau_1, \tau_2, \ldots, \tau_m\}$

Procedure:

Preprocessing & Coarse positioning

- Extract envelope signals $E(t)$ from $I(t)$
- Locate coarse change-point indices r:r=argmax$_t$(d$E(t)$ / dt)
- Search interval compression

  Define narrowed search intervals R=[r-l,…, r,…,r+l] centered at r

  Extract subsequences $X = I(R)$
- $start \leftarrow r - l$; $end \leftarrow r + l$

Function CPD(X, $start$, end, P, L_{min}):

For τ in range($start$+1, end)

Compute the gain $Gain(\tau)$:

IF $Gain(\tau) > Gain_{\max}$

Set $\tau^* \leftarrow \tau$

Set $Gain_{\max} \leftarrow Gain(\tau)$

III. Experiment Results and Discussion

A. Experiment setup

Fig. 3 illustrates the experimental setup of the fiber BP positioning method with a 101 km long fiber link. The fiber lengths involved at typical of realistic scenarios, and do not reflect the maximum length possible. The bidirectional fiber link is constructed using four spools of single-mode fiber (SMF) with FC/APC connections. SMF1 and SMF2 serve as the link from transceiver 1 to transceiver 2, with lengths of 50.544 km and 50.564 km, respectively. Similarly, SMF3 and SMF4 form the link in the opposite direction (from transceiver 2 to transceiver 1), with matching lengths of 50.544 km and 50.564 km. To compensate for the propagation loss of the long fiber link, two EDFAs (Thorlabs EDFA100S) were inserted into the two transmission directions. During all measurements, both EDFAs were operated with a fixed pump-current setting. Therefore, the abrupt input-power reduction caused by the fiber break is preserved more directly at the amplifier output. Both transceiver units are equipped with a distributed feedback laser (DFB) as laser source, an oscilloscope (OSC), and a photodetector (PD). The center wavelengths of the two DFB lasers are set to 1550.52 nm (DFB1) and 1549.72 nm (DFB2). This wavelength assignment is used to emulate the separate uplink and downlink channels which composed of two parallel fiber links for bidirectional data transmission. In the experiment, owing to the superior extinction ratio of the acousto-optic modulator (AOM), it was employed to simulate a clean fiber break event. To ensure that the optical intensities in both directions vanish simultaneously and at the same location, two dense wavelength division multiplexers (DWDMs) were used to combine the bidirectional optical paths into a single path through the AOM. Thus, both the simulated (ideal experiment, for calibration) BP and the FTB consist of two DWDMs and one AOM. In Transceiver 2, the source is followed by an intensity modulator (IM), which performs on-off keying (OOK) modulation on the continuous-wave optical carrier for transmitting communication signals. The electrical signals for OOK modulation were generated using an arbitrary waveform generator (AWG).

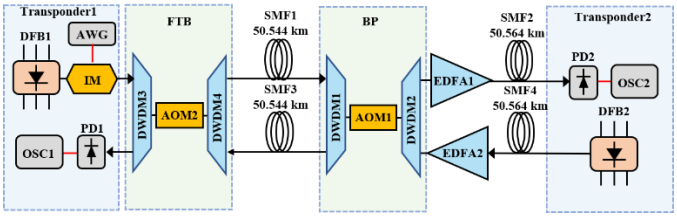


Fig. 3. Experimental configuration of fiber break point positioning method based on forward transmission; DFB: distributed feedback laser, AOM: acousto-optic modulator, IM: intensity modulator, AWG: arbitrary waveform generator, SMF: single mode fiber, DWDM: dense wavelength division multiplexer, OSC: oscilloscope, FTB: Fiber Termination Box; BP: Fiber break point, PD: Photodetector, EDFA: erbium-doped fiber amplifier.

B. Break point positioning under OOK modulation

Fig. 4 displays the optical signal of the 75 Mbps PRBS7 pseudo-random bit sequence acquired by OSC1 at the transceiver 1. The sampling rate of OSC1 was set to 2.5 GS/s. The time-domain waveform of the optical communication signal after DC removal and low-pass filtering is shown in Fig. 4 (a). As shown in the figure, within the 400 ns acquisition period, the communication signal recovered through threshold decision (threshold = 0 V) matches the modulated signal at the transmitter, with no bit errors observed. The eye diagram of the OOK modulated signal is shown in Fig. 4 (b). Due to the non-integer relationship between the oscilloscope sampling rate and the communication signal bit rate, clock recovery and resampling were applied to the intensity signal, resulting in 16 samples per unit interval. As presented in Fig. 4 (b), the eye width is 0.87 UI, the eye height is 3.32 mV, and the Q-factor is 6.38. The corresponding bit error rate (BER), calculated from this Q-factor, is 9×10^{-11}, indicating that the communication signal essentially meets the required performance specifications.

Authorized licensed use limited to: SHENZHEN UNIVERSITY. Downloaded on November 16,2026 at 08:26:42 UTC from IEEE Xplore. Restrictions apply.
© 2026 IEEE. All rights reserved, including rights for text and data mining and training of artificial intelligence and similar technologies. Personal use is permitted, but republication/redistribution requires IEEE permission. See https://www.ieee.org/publications/rights/index.html for more information.

This article has been accepted for publication in Journal of Lightwave Technology. This is the author's version which has not been fully edited and content may change prior to final publication. Citation information: DOI 10.1109/JLT.2026.3748590

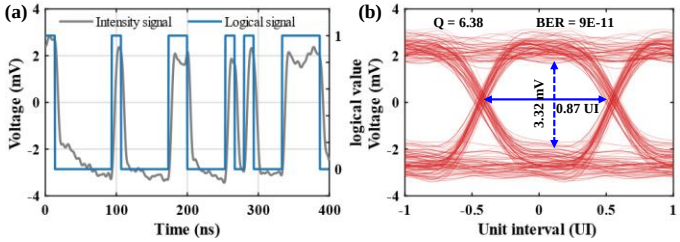


Fig. 4. Optical signal of the 75 Mbps pseudo-random bit sequence: (a) Intensity signal (gray) received by the photodetector at transceiver1 and the recovered communication logical signal (blue); (b) Eye diagram of the OOK modulated signal. UI: Unit interval, Q: Q factor, BER: Bit error rate calculated based on the Q-factor.

Fiber BP positioning experiments were performed under identical optical communication signal modulation conditions. In the experiments, two oscilloscopes (PicoScope 6426E) were used for data acquisition at the two ends. Both oscilloscopes were connected to the same host computer and controlled by a LabVIEW VI program. The acquisition routine for each oscilloscope was implemented as a separate non-reentrant sub-VI to ensure independent and uninterrupted streaming acquisition via USB 3.0. It should be emphasized that no external hardware trigger was used to synchronize the start of acquisition between the two oscilloscopes. Instead, both units shared a common 10 MHz external clock reference to calibrate their internal timebases. Under this configuration, each oscilloscope continuously streams data to the host computer without any data loss during the acquisition period. The start-time order of the two oscilloscopes was not fixed. The corresponding process of the fiber BP positioning method are presented in Fig. 5. To reduce computational complexity for subsequent positioning, the sampling rate of the oscilloscope was further reduced to 19.53 MS/s. During acquisition, the intensity signals were stored in segments, with each signal segment containing 1 M points. In Fig. 5, the time axes of signals from OSC1 and OSC2 are referenced to their respective acquisition start times t_{s1} and t_{s2}. Fig. 5 (a) and (b) display the intensity signals $I_1(t)$ and $I_2(t)$ (captured by the oscilloscopes at transceiver1 and transceiver2, respectively) containing the moment of intensity loss, along with their corresponding upper-peak envelopes $E_1(t)$ and $E_2(t)$ calculated with a peak sampling interval of 2000 points. The initial times of the two signals are the acquisition start times t_{s1} and t_{s2} of OSC1 and OSC2, respectively. Envelope extraction serves two purposes: first, it smooths the intensity signal; secondly, it suppresses high-frequency modulation components. This step is crucial to prevent the subsequent derivative operation from erroneously attributing the maximum derivative to logic-level transitions (e.g., '0' states) rather than to the actual envelope variation. The derivative curves of envelopes $E_1(t)$ and $E_2(t)$ are shown in Figs. 5 (c) and (d), respectively. As anticipated, a single extremum was observed in each signal segment, indicating its correspondence with the vicinity of the intensity loss moment. The index of this extremum in each signal segment serves as the center point. By defining a coarse range l of 5,000 points around each center, an optimal search interval for change-point detection is established. By performing optimal change-point detection function within each optimized search interval, the precise timing τ^* of intensity loss for every signal segment can be determined, which is the position of the red dot in Fig. 5 (e) and (f). Fig. 5 (e) presents the change-point detection results within the two optimized search intervals for the FTB break moment t_{c1} and the fiber break moment t_{b1} of intensity signal $I_1(t)$. The detected moments were determined to be 2.65127619 s for t_{c1} and 10.57667758 s for t_{b1}.

Similarly, detection of the change points corresponding to t_{c2} and t_{b2} were performed within their respective optimized search intervals for signal $I_2(t)$, with the results shown in Fig. 5 (f). The detected moments were determined to be 2.41968579 s for t_{c2} and 10.34459218 s for t_{b2}. By confining the search to an optimized interval, the algorithm achieves precise change-point position near its center, significantly refining the initial coarse estimate. Hence, with the values of Δt_1 and Δt_2 assigned as $t_{c1} - t_{c2}$ = 231.59 ms and $t_{b1} - t_{b2}$ = 232.09 ms, respectively, the BP position is calculated to be 50.551 km using eq. (6). This excellent agreement, with a mere 7 m deviation from the true position of 50.544 km, validates the feasibility of the proposed method for practical fiber BP positioning. The BP was placed at approximately the mid-point (50.544 km from transceiver 1) for experimental convenience. However, the proposed positioning formula (Eq. (6)) is independent of the break position Z. The same accuracy would be expected for a break at any position, as long as the intensity-loss moments can be reliably detected at both ends. Furthermore, in the experimental setup shown in Fig. 3. The EGO-CPD algorithm correctly deduced the calibration time instants t_{c1} and t_{c2} on the time axis, which demonstrates that the method can calculate BP even when they occur at either extreme of the fiber link.

To evaluate the repeatability of the fiber BP positioning method, successive measurements were conducted, with the positioning results shown in Fig. 6. First, following the configuration illustrated in Fig. 3, 20 repeated trials were performed using two DWDM and an AOM to emulate the BP. In this work, the positioning accuracy is defined as the root mean square error (RMSE) relative to the true break position, which accounts for both systematic bias and random fluctuations, while the standard deviation (STD) is used to characterize measurement repeatability. The results, presented in Fig. 6 (a), show a mean position value of 50.548 km with a standard deviation (STD) of 11.6 m over the 20 trials. The root mean square error (RMSE) relative to the actual BP position of 50.544 km is 12.1 m. Subsequently, to further verify the effectiveness of the BP positioning method, the AOM in Fig. 3 was replaced with an 0.5 m long single-mode fiber connecting two DWDMs. This fiber was then physically broken into two ends to simulate a real fiber break event, with 10 repeated trials carried out under this setup. The localization results, presented in Fig. 6 (b), show a mean value of 50.549 km with a STD of 6.1 m. The RMSE relative to the actual BP position of 50.544 km is 8.0 m. These results demonstrate the high accuracy and excellent repeatability of the proposed positioning method under both simulated (ideal experiment) and realistic fiber break conditions. It should be noted that the experimental system employed two different wavelengths,

Authorized licensed use limited to: SHENZHEN UNIVERSITY. Downloaded on November 16,2026 at 08:26:42 UTC from IEEE Xplore. Restrictions apply.
© 2026 IEEE. All rights reserved, including rights for text and data mining and training of artificial intelligence and similar technologies. Personal use is permitted, but republication/redistribution requires IEEE permission. See https://www.ieee.org/publications/rights/index.html for more information.

This article has been accepted for publication in Journal of Lightwave Technology. This is the author's version which has not been fully edited and content may change prior to final publication. Citation information: DOI 10.1109/JLT.2026.3748590

1550.52 nm and 1549.72 nm, for the two transmission directions over parallel fiber paths, indicating that the proposed method is applicable to bidirectional links with propagation-delay asymmetry when the effective group delay is properly calibrated.

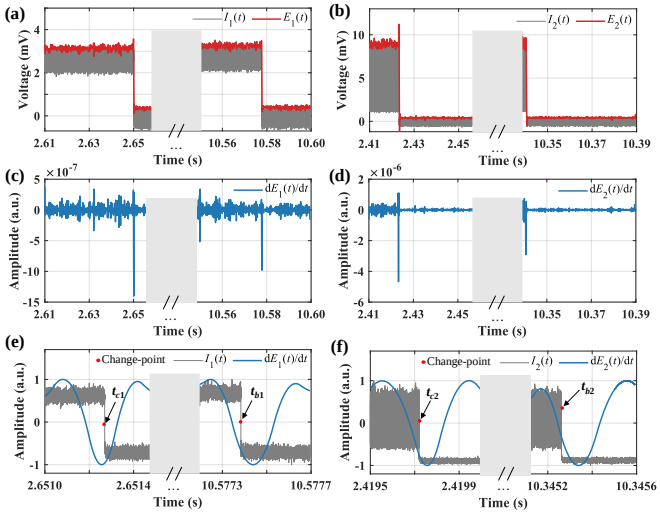


Fig. 5. Sequence of intermediate results for fiber BP positioning: (a) Intensity signal segment $I_1(t)$ and its envelope curve $E_1(t)$ (red), including the FTB break moment t_{c1} and fiber break moment t_{b1}. The signal start time is defined as the acquisition start time t_{s1} of OSC1 plus 2.61 s; (b) Intensity signal segment $I_2(t)$ and its envelope curve $E_2(t)$ (red), including the FTB break moment t_{c2} and fiber break moment t_{b2}. The signal start time is defined as the acquisition start time t_{s2} of OSC 2 plus 2.41 s; Derivative of (c) $E_1(t)$; (d) $E_2(t)$; Position of the change-point τ^* (position of the red dot) detected by the EGO-CPD algorithm in signal (e) $I_1(t)$; (f) $I_2(t)$.

To further evaluate the reproducibility of the calibration process, Fig. 6 (c) and 6 (d) plot the calibrated time offset Δt_1 against the positioning deviation for the AOM-emulated break and the real fiber break experiments, respectively. A positive Δt_1 indicates that OSC1 started acquisition before OSC2. In the AOM experiments, two different acquisition-start configurations resulted in two distinct Δt_1 groups centered at approximately −0.23 s and 0.23 s. The within-group variations were approximately 8.0 ms and 14.3 ms, respectively. Despite the large shift in Δt_1 between the two groups, no corresponding systematic shift in the estimated break position was observed. In the physical fiber-break experiments, Δt_1 was intentionally varied over a range of approximately 5.8 s, while the positioning deviation remained within a peak-to-peak range of approximately 20.9 m. These results demonstrate that the positioning result is insensitive to the absolute acquisition-time offset between the two oscilloscopes, because the common timing offset is removed through the calibration term in Eq. (6). The remaining positioning fluctuations are mainly associated with the uncertainty in determining the intensity-loss moments and other experimental fluctuations.

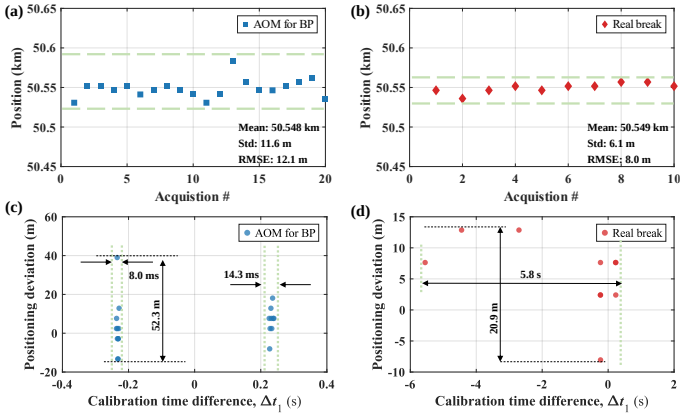


Fig. 6. Repeatability of fiber BP positioning: (a) Results of 20 repeated positioning trials using an AOM as ideal BP; (b) Results of 10 repeated positioning trials using cut single-mode fiber as realistic BP; (c) Relationship between acquisition-time offset Δt_1 and the positioning deviation for the AOM trials; (d) Relationship between Δt_1 and the positioning deviation for the real fiber break trials. Std: standard deviation; RMSE: Root mean square error, Mean: Mean value of position.

C. Comparison of change point detection algorithms

To demonstrate the effectiveness of the EGO-CPD algorithm, its performance is compared with other four widely used CPD methods, as shown in Table 1. The compared methods are PELT [23], binary segmentation (Binseg) [24], Window and BottomUp [25]. These 5 methods were evaluated using the same dataset of 20 fiber BP experiments. To reduce computational time, all 5 methods were applied within an optimized search space guided by the maximum derivative, with a fixed interval length of 10,000 points. The computations were performed on a computer equipped with an Intel® Xeon® W-1370 CPU. The comparative experiment was assessed based on the Std and RMSE of the calculated positions relative to the ground truth value, as well as the average computation time. As shown in Table 1, among the 5 CPD methods, EGO-CPD, PELT, and BinSeg achieved identical—and the lowest—Std and RMSE values. In fact, these 3 methods produced completely consistent results across all 20 datasets. In terms of computation time, the EGO-CPD method required 2.39 s, which is only 0.20 s longer than the fastest method, Bottom-Up. These results demonstrate that the proposed method EGO-CPD not only delivers high positioning accuracy, but also maintains low computational overhead. The high execution time of PELT observed in Table I is mainly attributed to its dynamic-programming search for a general multiple-change-point partition, in which every sample is considered as a candidate segment boundary.

Authorized licensed use limited to: SHENZHEN UNIVERSITY. Downloaded on November 16,2026 at 08:26:42 UTC from IEEE Xplore. Restrictions apply.
© 2026 IEEE. All rights reserved, including rights for text and data mining and training of artificial intelligence and similar technologies. Personal use is permitted, but republication/redistribution requires IEEE permission. See https://www.ieee.org/publications/rights/index.html for more information.

This article has been accepted for publication in Journal of Lightwave Technology. This is the author's version which has not been fully edited and content may change prior to final publication. Citation information: DOI 10.1109/JLT.2026.3748590

TABLE I
PERFORMANCE COMPARISON OF FIVE DIFFERENT CHANGE POINT DETECTION METHODS IN FIBER BP POSITIONING.

	EGO-CPD (this work)	PELT	Binseg	Window	BottomUp
Positioning Std (m)	**11.3**	**11.3**	**11.3**	17.3	22.6
Positioning RMSE (m)	**12.1**	**12.1**	**12.1**	18.4	23.1
Computation time (s)	2.39	1864.67	3.89	2.68	**2.19**

D. Break point positioning with commercial optical transceivers

In order to realistically emulate an in-line fiber break during real-time data transmission, a bidirectional optical path was implemented using gigabit commercial optical transceivers (TP-LINK, TL-FC311A-60 and TL-FC311B-60). The experimental setup is shown in Fig. 7. The forward path (1490 nm) from transceiver1 traverses OC1, the FTB, and a cascaded fiber link comprising SMF1 (9.760 km) and SMF2 (20.075 km), with a 0.5 m length single-mode fiber serving as the inter-spool connection. The BP was thus located at 9.760 km. The signal was then split by OC2 to transceiver2 and PD2, with the latter being monitored in real time by OSC2. The return path (1550 nm from transceiver2) was monitored by OSC1. To reduce the computational load, the sampling rate of the oscilloscope was set to 19.53 MS/s. The actual break event was simulated by severing the 0.5 m length connection fiber. Additionally, the FTB disconnection/connection cycle was carried out by cutting and subsequently replacing the single-mode fiber between OC1 and SMF1.

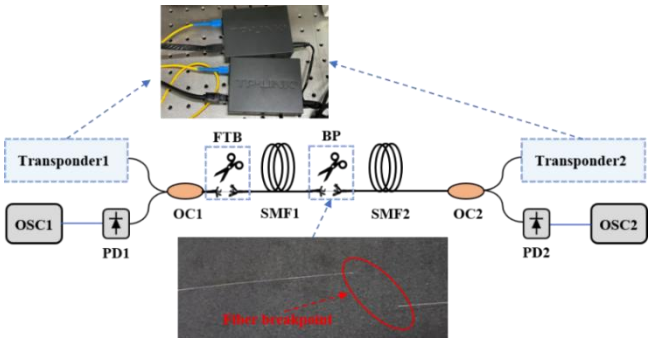


Fig. 7. Experiment setup for emulating a real fiber-break scenario using gigabit commercial optical transceivers. OC: Optical couple, PD: Photodetector. SMF: single mode fiber.

The experimental results of fiber BP positioning are presented in Fig. 8. The detection of the intensity loss moments, t_{c1} and t_{c2}, corresponding to the disconnection of the FTB, is shown in Fig. 8 (a) and (c), respectively. The time zero in each plot was set to t_{s1} and t_{s2} corresponding to the start of acquisition for OSC1 and OSC2, respectively. In Fig. 8 (a), t_{c1} occurred at 6.58043689 s. Similarly, in Fig. 8(c), t_{c2} is located at 6.80595942 s. The detection of the intensity loss moments, t_{b1} and t_{b2}, associated with the actual BP, is displayed in Fig. 8 (b) and (d). t_{b1} in Fig. 8(b) was found at 82.47373389 s, while t_{b2} in Fig. 8(d) is 82.69916109 s. From these measurements, the time differences are calculated as $\Delta t_1 = t_{c1} - t_{c2}$ = -225,522.53 μs and $\Delta t_2 = t_{b1} - t_{b2}$ = -225,427.20 μs. Substituting Δt_1 and Δt_2 into Eq. (6) gives a BP position of 9.736 km. This result deviates by only 24 m from the actual position of 9.760 km, thus indicating that the positioning method maintains high accuracy under conditions that simulate practical deployment.

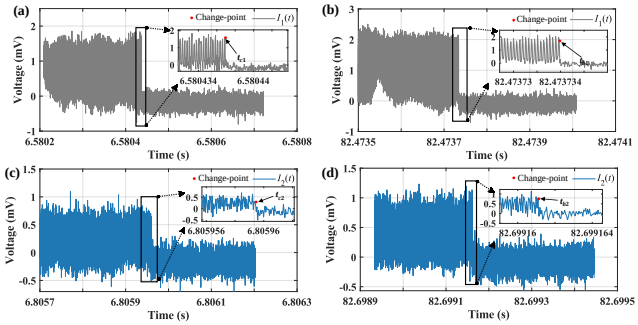


Fig. 8. Experiment results of the BP positioning method under real signal transmission conditions, for: (a) t_{c1}; (b) t_{b1}; (c) t_{c2}; and (d) t_{b2}.

Finally, we investigated the influence of received optical power (ROP) and optical signal-to-noise ratio (OSNR) on the positioning accuracy of fiber BPs. The experimental results are shown in Fig. 9. To avoid stimulated Brillouin scattering (SBS) induced by high optical power over long propagation distances, and to facilitate reliable measurements, the maximum ROP was set to –7.4 dBm, and the pseudo-random bit sequence modulation was turned off. Nine different received power levels were tested from high to low, with an interval of approximately 1 dBm between adjacent levels. The fiber BP was fixed at 50.210 km, and 20 repeated measurements were taken at each power level. In Fig. 9, the BP position obtained from individual trials are represented by triangles. For each ROP gradient, the mean BP position calculated from 20 repeated measurements is indicated by a red circle. The range of one standard deviation above and below the mean is shown as a purple rectangle, and the polynomial fitting curve of the mean values is displayed as a purple dashed line. As can be seen, at the highest ROP (–7.4 dBm), the positioning STD is 3.1 m. When the ROP drops to –16.6 dBm, the STD still remains 7.6 m. Furthermore, the equivalent optical signal-to-noise ratio (OSNR) was estimated from the temporal intensity fluctuations of the unmodulated received optical signal. Under the signal–ASE-beat-noise-dominant approximation, the OSNR was calculated as [27]:

$$\mathrm{OSNR} = 10\log_{10}\left(\frac{2V_{\mathrm{DC}}^2}{\sigma_V^2}\right) + 10\log_{10}\left(\frac{B_e}{B_{\mathrm{ref}}}\right), \qquad (10)$$

where B_{ref} = 12.5 GHz corresponds to the conventional 0.1 nm reference bandwidth around 1550 nm, and B_e = 1 GHz is the effective electrical bandwidth determined by the oscilloscope. After correcting the bandwidth normalization, the equivalent OSNR at the lowest ROP is approximately 6.13 dB. The positioning STD remains 7.6 m under this condition, demonstrating the robustness of the proposed BP positioning method at low received optical power.

Authorized licensed use limited to: SHENZHEN UNIVERSITY. Downloaded on November 16,2026 at 08:26:42 UTC from IEEE Xplore. Restrictions apply.
© 2026 IEEE. All rights reserved, including rights for text and data mining and training of artificial intelligence and similar technologies. Personal use is permitted, but republication/redistribution requires IEEE permission. See https://www.ieee.org/publications/rights/index.html for more information.

This article has been accepted for publication in Journal of Lightwave Technology. This is the author's version which has not been fully edited and content may change prior to final publication. Citation information: DOI 10.1109/JLT.2026.3748590

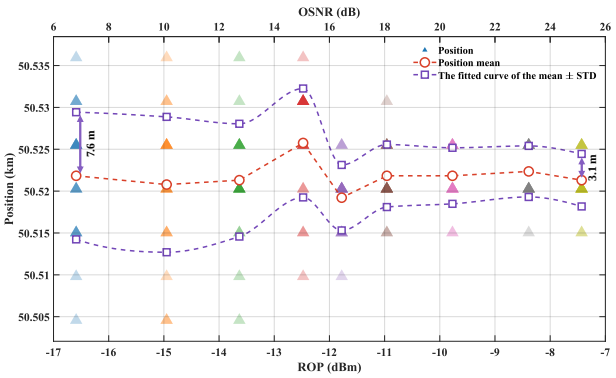


Fig. 9. Influence of received optical power (ROP) and optical signal-to-noise ratio (OSNR) on the standard deviation (STD) of fiber BP position.

IV. Discussion

In order to hold a balanced evaluation against existing monitoring solutions, a comparison of the proposed method is made with existing fiber fault positioning techniques. Conventional OTDR can achieve sub-meter positioning accuracy but requires a dedicated laser source and detector, operates out-of-service (or occupies a separate wavelength), and its distance is limited by backscattering to typically less than 100 km. Bidirectional repeater-amplified Φ-OTDR systems [12] also offer sub-meter accuracy, yet they necessitate coherent receivers and modifications to the existing repeater infrastructure, making deployment costly. WDM-based Φ-OTDR sensing approaches [15] integrate sensing and communication by allocating a dedicated wavelength channel. However, this reduces the available communication bandwidth and increases system complexity. The bit-counting forward method [18,19] uses virtually no additional hardware and does not occupy communication bandwidth, but its positioning accuracy is on the order of hundreds of meters. In contrast, the method proposed in this work achieves a positioning accuracy (RMSE) of 8.0 m (STD of 6.1 m) without requiring significant hardware changes nor separate wavelength. Beyond the experimentally demonstrated 101 km fiber link, the use of forward-transmitted optical signals provides the potential for extending the positioning distance through optical amplification. Cascaded EDFAs can compensate for fiber attenuation and preserve sufficient received optical power for detecting the intensity-loss event. Thus, the proposed approach offers a favorable trade-off between accuracy, cost, and scalability for break-point positioning in long-haul optical backbone networks. For ultra-long-haul transmission, chromatic dispersion is another important factor affecting the positioning performance. The accumulated dispersion produces different group delays among the spectral components of the transmitted optical signal, which may broaden and smooth the falling edge associated with the fiber-break event. Therefore, the practical positioning range is jointly limited by the received optical power, accumulated ASE noise, chromatic dispersion, signal bandwidth, receiver bandwidth, and other transmission impairments. Dispersion compensation or dispersion-aware signal processing may alleviate these effects, while a quantitative determination of the maximum positioning range requires further long-haul transmission simulations and experiments.

The relative timebase stability of the two acquisition systems is an important factor for long-term operation of the proposed positioning method. In the present experiment, the two oscilloscopes were operated without a common hardware trigger, and therefore their acquisition start times were asynchronous. However, both oscilloscopes were referenced to the same 10 MHz external clock to stabilize their internal timebases. The timing errors of two independent acquisition systems can generally be separated into an initial time offset and a relative clock-frequency error. The former is compensated by the calibration term Δt_1, whereas the latter may lead to an accumulated timebase drift after calibration. If the relative fractional frequency error between the two acquisition systems is denoted as $\Delta\Psi$, the accumulated timing error after an elapsed time T, can be approximated as $\Delta\Psi T$. According to Eq. (6), this timing drift produces an additional positioning error of $c\Delta\Psi T/2n$, Therefore, when two free-running clocks are used, the localization accuracy can gradually degrade with increasing time after calibration unless the relative clock-frequency offset is sufficiently small or appropriately compensated. In the present experiment, the common 10 MHz reference suppresses the relative frequency offset between the two oscilloscope timebases and therefore strongly reduces the accumulated timing drift during continuous acquisition. This also clarifies the meaning of "synchronization-free" in this work: synchronized acquisition start times or a common absolute timestamp are not required, whereas sufficient relative timebase stability is still necessary for long-term high-accuracy positioning.

For practical long-haul systems in which distributing a common frequency reference between geographically separated terminals is inconvenient, the relative timebase can alternatively be calibrated by jointly estimating the clock offset and clock skew, which can be estimated from multiple common timing observations using regression or estimation-based clock calibration methods [29].

V. Conclusion

In summary, to overcome limitations in conventional fiber break point (BP) detection systems such as OTDR-based systems, namely dedicated hardware, bandwidth and pulse distortion issues, this work proposes a new fiber BP positioning method based on the time difference of intensity-loss moments in bidirectionally transmitted optical communication signals. It requires minimal additional hardware (simple photodetector and data acquisition module) to the existing communication infrastructure. Combined with a synchronization-free method and a new change-point detection algorithm, this approach is demonstrated in both simulated and more realistic fiber break scenarios. The experimental results show that in a 100 km bidirectional link using an AOM to emulate a clean fiber break, the proposed method achieves an RMSE of 12.1 m and an STD of 11.6 m. For the physical fiber-break experiments, an RMSE of 8.0 m

Authorized licensed use limited to: SHENZHEN UNIVERSITY. Downloaded on November 16,2026 at 08:26:42 UTC from IEEE Xplore. Restrictions apply.
© 2026 IEEE. All rights reserved, including rights for text and data mining and training of artificial intelligence and similar technologies. Personal use is permitted, but republication/redistribution requires IEEE permission. See https://www.ieee.org/publications/rights/index.html for more information.

This article has been accepted for publication in Journal of Lightwave Technology. This is the author's version which has not been fully edited and content may change prior to final publication. Citation information: DOI 10.1109/JLT.2026.3748590

was achieved. Furthermore, fiber BP experiments conducted with commercial optical transceivers yield a positioning error of only 24.0 m. The proposed approach provides a new direction for intelligent monitoring of long-haul optical backbone networks. Furthermore, the positioning range of the proposed method has the potential to be further extended through techniques such as optical amplification, dispersion compensation, and optimization of the transmission and detection schemes.

DISCLOSURES

The authors declare no conflicts of interest.

REFERENCES

[1] J. Simão and L. Veiga, "A Taxonomy of Adaptive Resource Management Mechanisms in Virtual Machines: Recent Progress and Challenges," *in Cloud Computing: Principles, Systems and Applications*, N. Antonopoulos and L. Gillam Eds. Cham: Springer International Publishing, 2017, pp. 59-98.

[2] L. Atzori, A. Iera, and G. Morabito, "The Internet of Things: A survey," *Computer Networks*, vol. 54, no. 15, pp. 2787-2805, 2010, doi: 10.1016/j.comnet.2010.05.010.

[3] S. M. LaValle, *Virtual Reality*. Cambridge: Cambridge University Press, 2023.

[4] A. Liu et al., "Deepseek-v3 technical report," *arXiv preprint arXiv:2412.19437*, 2024.

[5] M. M. Rad, K. Fouli, H. A. Fathallah, L. A. Rusch, and M. Maier, "Passive optical network monitoring: challenges and requirements," *IEEE Communications Magazine*, vol. 49, no. 2, pp. s45-S52, 2011, doi: 10.1109/MCOM.2011.5706313.

[6] T. Xie, C.-C. Zhang, B. Shi, Z. Chen, and Y. Zhang, "Integrating distributed acoustic sensing and computer vision for real-time seismic location of landslides and rockfalls along linear infrastructure," *Landslides*, vol. 21, no. 8, pp. 1941-1959, 2024, doi: 10.1007/s10346-024-02268-y.

[7] E. F. Williams et al., "Distributed sensing of microseisms and teleseisms with submarine dark fibers," *Nature Communications*, vol. 10, no. 1, p. 5778, 2019, doi: 10.1038/s41467-019-13262-7.

[8] M. Ma et al., "Joint break-point localization sensing based on OFDR and non-disruptive communication fiber ISAC system," *Optics & Laser Technology*, vol. 192, p. 113726, 2025, doi: 10.1016/j.optlastec.2025.113726.

[9] J. Gagnon, "The Fundamentals of an OTDR," *Optical Business Unit*, 2008.

[10] N. Nakao, H. Izumita, T. Inoue, Y. Enomoto, N. Araki, and N. Tomita, "Maintenance Method Using 1650-nm Wavelength Band for Optical Fiber Cable Networks," *J. Lightwave Technol.*, vol. 19, no. 10, p. 1513, 2001.

[11] L. Han, X. Zhang, and J. He, "A multi-function and high precision submarine optical fiber monitor," in *AOPC 2017: Fiber Optic Sensing and Optical Communications*, 2017, vol. 10464: SPIE, pp. 503-507.

[12] C. Fan et al., "300 km ultralong fiber optic DAS system based on optimally designed bidirectional EDFA relays," *Photon. Res.*, vol. 11, no. 6, pp. 968-977, 2023, doi: 10.1364/PRJ.485701.

[13] H. He et al., "Integrated sensing and communication in an optical fibre," *Light: Science & Applications*, vol. 12, no. 1, p. 25, 2023, doi: 10.1038/s41377-022-01067-1.

[14] L. Gu et al., "Co-wavelength-channel integration of ultra-low-frequency distributed acoustic sensing and high-capacity communication," *Photon. Res.*, vol. 13, no. 6, pp. 1611-1619, 2025, doi: 10.1364/PRJ.551958.

[15] M. F. Huang et al., "First Field Trial of Distributed Fiber Optical Sensing and High-Speed Communication Over an Operational Telecom Network," *J. Lightwave Technol.*, vol. 38, no. 1, pp. 75-81, 2020, doi: 10.1109/JLT.2019.2935422.

[16] Y. Yan, F. N. Khan, B. Zhou, A. P. T. Lau, C. Lu, and C. Guo, "Forward Transmission Based Ultra-Long Distributed Vibration Sensing With Wide Frequency Response," J. Lightwave Technol., vol. 39, no. 7, pp.2241-2249, 2021. [Online].

[17] M. Chen et al., "Distributed Vibration Sensing Based on a Forward Transmission Polarization-Generated Carrier," *Sensors*, vol. 24, no. 16, p. 5257, doi: 10.3390/s24165257.

[18] P. Rosher, S. Fenning, P. Cochrane, and A. Hunwicks, "An automatic optical fibre break location scheme for duplex and diplex transmission systems," *British Telecom technology journal*, vol. 6, no. 1, pp. 54-59, 1988.

[19] S. Zemon, A. Budman, T. Wei, E. Eichen, and K. T. Ma, "Decay of transmitted light during fiber breaks-implications for break location," *J. Lightwave Technol.*, vol. 12, no. 9, pp. 1532-1535, 1994, doi: 10.1109/50.320934.

[20] G. Y. Chen et al., "Intrinsic distributed sensing using wavelength-multiplexed QPSK signals in fiber-optic communication," *Opt. Express*, vol. 34, no. 2, pp. 1510-1521, 2026, doi: 10.1364/OE.584647.

[21] L. Han, J. Li, R. Lu, X. Chen, and H. Li, "Inter-satellite distributed time synchronization solution with nanosecond accuracy in satellite networks," *Opt. Express*, vol. 33, no. 7, pp. 14555-14565, 2025, doi: 10.1364/OE.543159.

[22] X. Zhu et al., "Robust fiber-based frequency synchronization system immune to strong temperature fluctuation," *Chin. Opt. Lett.*, vol. 16, no. 1, p. 010605, 2018, doi: 10.1364/COL.16.010605.

[23] Z. Liu, W. Lu, J. Wu, S. Yang, and G. Li, "A PELT-KCN Algorithm for FMCW Radar Interference Suppression Based on Signal Reconstruction," *IEEE Access*, vol. 8, pp. 45108-45118, 2020, doi: 10.1109/ACCESS.2020.2977098.

[24] C. Li, Y. Lei, L. Guo, E. Zio, H. Gao, and B. Yang, "GMM-BinSeg: A Data Segmentation Method for CFRP/Aluminum Stacks Drilling–Countersinking Monitoring Signal," *IEEE Transactions on Instrumentation and Measurement*, vol. 73, pp. 1-10, 2024, doi: 10.1109/TIM.2024.3374301.

[25] C. Truong, L. Oudre, and N. Vayatis, "Selective review of offline change point detection methods," *Signal Processing*, vol. 167, p. 107299, 2020, doi: https://doi.org/10.1016/j.sigpro.2019.107299.

[26] W. I. Way and Y. W. Lai, "Effect of transient gain compression in a saturated EDFA on OTDR testing," *in Conference on Optical Fiber Communication, San Jose, California*, 1994, vol. 4: Optica Publishing Group, in 1994 OSA Technical Digest Series, p. WC1, doi: 10.1364/OFC.1994.WC1.

[27] G. P. Agrawal, *Fiber-optic communication systems*. Wiley-interscience New York, 2002.

[28] M. W. AlTaha, H. Jayatilleka, Z. Lu, J. F. Chung, D. Celo, D. Goodwill, E. Bernier, S. Mirabbasi, L. Chrostowski, and S. Shekhar, "Monitoring and automatic tuning and stabilization of a 2×2 MZI optical switch for large-scale WDM switch networks," *Opt. Express*, vol. 27, no. 17, pp. 24747–24764, 2019, doi: 10.1364/OE.27.024747.

[29] J. Elson, L. Girod, and D. Estrin, "Fine-grained network time synchronization using reference broadcasts," SIGOPS Oper. Syst. Rev., vol. 36, no. SI, pp. 147–163, 2003, doi: 10.1145/844128.844143.

Shangwei Dai was born in Guangxi, China, in 1998. He received his Master's degree in Electronic Information from the Shantou University, Shantou, China, in 2023 and the Ph.D. degree in Optical Engineering from Shenzhen University, Shenzhen, China, in 2026. He is currently a Postdoctoral Researcher at Shenzhen University. His current research interests focus on super long-range distributed vibration sensors based on phase-sensitive forward DAS.

Hanjie Liu received her PhD degree from the National Engineering Laboratory for Fiber Optic Sensing Technology, Wuhan University of Technology, China in 2024. At present, she is a postdoctoral fellow at Shenzhen University, Shenzhen, China. Her research direction is distributed fiber-optic vibration sensing and communication-sensing integration.

Xing Rao was born in Jiangxi, China, in 1998. He received the B.S. degree in optoelectronic information science and engineering from Nanchang Hangkong University, Nanchang,

Authorized licensed use limited to: SHENZHEN UNIVERSITY. Downloaded on November 16,2026 at 08:26:42 UTC from IEEE Xplore. Restrictions apply.
© 2026 IEEE. All rights reserved, including rights for text and data mining and training of artificial intelligence and similar technologies. Personal use is permitted, but republication/redistribution requires IEEE permission. See https://www.ieee.org/publications/rights/index.html for more information.

This article has been accepted for publication in Journal of Lightwave Technology. This is the author's version which has not been fully edited and content may change prior to final publication. Citation information: DOI 10.1109/JLT.2026.3748590

China, in 2020, and the Ph.D. degree from Shenzhen University, Shenzhen, China, in 2025. He is currently a Postdoctoral Researcher at Shenzhen University. His current research interests focus on integrated sensing and communication.

Danxia Lu received the B.S. degree in light sources and lighting from Guangdong Polytechnic Normal University, Guangzhou, China, in 2023 and the Master's degree from Shenzhen University, Shenzhen, China, in 2026. Her research interests include SDM distributed multi-parameter sensing based on phase-sensitive forward transmission of light.

Linqiao Du received his Master's degree in Electronic information from Henan normal university, Henan, China, 2024. He is now working toward a PhD degree in Shenzhen University. His current research interests focus on super long-range distributed vibration sensor based on Raman amplification.

Qiji Ma received Bachelor's degree in Electronic Information from Wuhan Institude of Technology, Hubei, China, 2025. He is now working toward a Master degree in Shenzhen University. His current research interests focus on muti-parameters optical fiber sensing utilizing forward propagating light.

Guoqiang Liu received the B.S. degree in Measurement and Control Technology and Instrumentation from Shenzhen University, Shenzhen, China, in 2024. He is currently pursuing the Ph.D. degree at Shenzhen University. His current research interests include fiber-optic sound source localization and long-distance distributed fiber-optic vibration sensing.

Junhong Lu received the B.S. degree in Electronic Information Engineering from Central China Normal University, China, in 2024. He is now working toward a Master degree in Shenzhen University. His current research interests in long-distance distributed fiber-optic vibration sensing.

George Y. Chen graduated with a 4-year MEng (Bachelor's and Master's joint degree) from Imperial College London in 2009, in the field of electronics and electrical engineering with computer science. He completed his PhD from the Optoelectronics Research Centre at the University of Southampton in 2013. He worked in an industrial research lab as a postdoctoral research fellow for SPI Lasers Ltd. from 2013 to 2015. He joined the University of South Australia as a research fellow in 2015, and senior research fellow in 2019. He joined Shenzhen University as a Professor in 2021. He is a Senior Member of Optica / IEEE.

Yiping Wang was born in Chongqing, China, in 1971. He received the B.Eng. degree in precision instrument engineering from Xi'an Institute of Technology, China, in 1995 and the M.S. degree and Ph.D. degree in optical engineering from Chongqing University, China, in 2000 and 2003, respectively. From 2003 to 2005, he was with Shanghai Jiao Tong University, China, as a Postdoctoral Fellow. From 2005 to 2007, he was with the Hong Kong Polytechnic University, as a Postdoctoral Fellow. From 2007 to 2009, he was with the Institute of Photonic Technology (IPHT), Jena, Germany, as a Humboldt Research Fellow. From 2009 to 2011, he was with the Optoelectronics Research Centre (ORC), University of Southampton, U.K., as a Marie Curie Fellow. Since 2012, he has been with Shenzhen University, Shenzhen, China, as a Distinguished Professor. His current research interests focus on optical fiber sensors, fiber gratings, and photonic crystal fibers. He has authored or coauthored 1 book, 21 patent applications, and more than 240 journal and conference papers. Prof. Wang is a Fellow of Optica and the Chinese Optical Society.

Junmin Liu received the B.S. and M.E. degrees in Computer Science and Technology from Hunan University, China, in 2010 and 2013, respectively, and the Ph.D. degree from Shenzhen University, China, in 2019. She is currently an associate professor at the College of New Materials and New Energies,Shenzhen Technology University. Her research primarily focuses on high-speed optical communication and optical computing technologies.

Guoxiang Xu serves as Technical Director at HMN TECHNOLOGIES GROUP CO.,LTD., leading R&D of submarine optical cable systems. He has developed large-core, high-capacity central tube-type cables and transoceanic repeater-equipped cables, with products passing 5000-meter depth certification tests in 2017 and 2023. His innovations have earned 80 UJ&UQJ certifications for submarine cable reliability. Mr. Xu's work advances deep-sea communication infrastructure, focusing on signal stability and durability in extreme marine environments.

Xu Rendong, Professor-level Senior Engineer, holds a PhD in Mechanical Engineering from Zhejiang University. He serves as General Manager of HMN TECHNOLOGIES GROUP CO.,LTD.. and Director of the Jiangsu Provincial Innovation Center for Marine Information Technology and Equipment. His research focuses on subsea communication, deep-sea equipment R&D and industrial operation. He also holds academic posts as the Chairman of two specialized committees under the Chinese Society for Imaging Science and Technology and Jiangsu marine societies, and the President of the Hainan Marine Society. He has led multiple national and provincial scientific projects. He has been awarded six Provincial and Ministerial First Prizes for Science and Technology.

Authorized licensed use limited to: SHENZHEN UNIVERSITY. Downloaded on November 16,2026 at 08:26:42 UTC from IEEE Xplore. Restrictions apply.
© 2026 IEEE. All rights reserved, including rights for text and data mining and training of artificial intelligence and similar technologies. Personal use is permitted, but republication/redistribution requires IEEE permission. See https://www.ieee.org/publications/rights/index.html for more information.